



1 **Geophysical fingerprint of the 4-11 July 2024 eruptive activity at 2 Stromboli volcano, Italy.**

3
4 Luciano Zuccarello^{1,2}, Duccio Gheri¹, Silvio De Angelis^{2,1}, Riccardo Civico³, Tullio Ricci³, Piergiorgio
5 Scarlato³.

6 1Istituto Nazionale di Geofisica e Vulcanologia, Sezione di Pisa, via Cesare Battisti, 53, 56125, Pisa, Italy.

7 2School of Environmental Sciences, University of Liverpool, 4 Brownlow Street, L69 3GP, Liverpool, UK.

8 3Istituto Nazionale di Geofisica e Vulcanologia, Sezione di Roma1, via di Vigna Murata, 605, 00143, Roma, Italy.

9 *Correspondence to:* Luciano Zuccarello (luciano.zuccarello@ingv.it); Duccio Gheri (duccio.gheri@ingv.it)

10 **Abstract.** Paroxysmal eruptions, characterized by sudden and vigorous explosive activity, are common events at many open-
11 vent volcanoes. Stromboli volcano, Italy, is well-known for its nearly continuous degassing activity and mild explosions from
12 the summit craters, occasionally punctuated by energetic, short-lived paroxysms. Here, we analyse multi-parameter
13 geophysical data recorded at Stromboli in early July 2024, during activity that led to a paroxysmal eruption on 11 July. We
14 use seismic, infrasound and ground deformation data, complemented by visual and Unoccupied Aircraft System observations,
15 to identify key geophysical precursors to the explosive activity and reconstruct the sequence of events. Elevated levels of
16 volcanic tremor and Very Long Period (VLP) seismicity accompanied moderate explosive activity, lava emission and small
17 collapses from the north crater, leading to a major explosion on 4 July, 2024 at 12:16 (UTC). Collapse activity from the North
18 crater area continued throughout July 7, while effusive activity occurred from two closely-spaced vents located on the Sciara
19 del Fuoco slope, on the Northwest flank of the volcano. On 11 July, a rapid increase in ground deformation preceded, by
20 approximately 10 minutes, a paroxysmal event at 12:08 (UTC); the explosion produced a 5 km-high eruptive column and
21 pyroclastic density currents along Sciara del Fuoco. We infer that the early activity in July was linked to eruption of resident
22 magma within the shallowest parts of the volcano plumbing. This was followed by lowering of the magma level within the
23 conduit system as indicated by the location of newly opened effusive vents. The rapid inflation observed before the paroxysmal
24 explosion on 11 July is consistent with the rapid expansion of gas-rich magma rising from depth, as frequently suggested at
25 Stromboli during energetic explosive events. Our results provide additional valuable insights into the eruptive dynamics of
26 Stromboli and other open-conduit volcanoes, and emphasize the importance of integrated geophysical observations for
27 understanding eruption dynamics, their forecasting and associated risk mitigation.

28 **1 Introduction**

29 Stromboli is an open conduit stratovolcano located in the Tyrrhenian Sea, off the northern coast of Sicily; its activity is
30 characterized by continuous degassing and frequent, small-to-moderate, explosions occurring every few minutes from the
31 summit craters, the well-known Strombolian activity. However, activity at Stromboli can rapidly escalate into more energetic

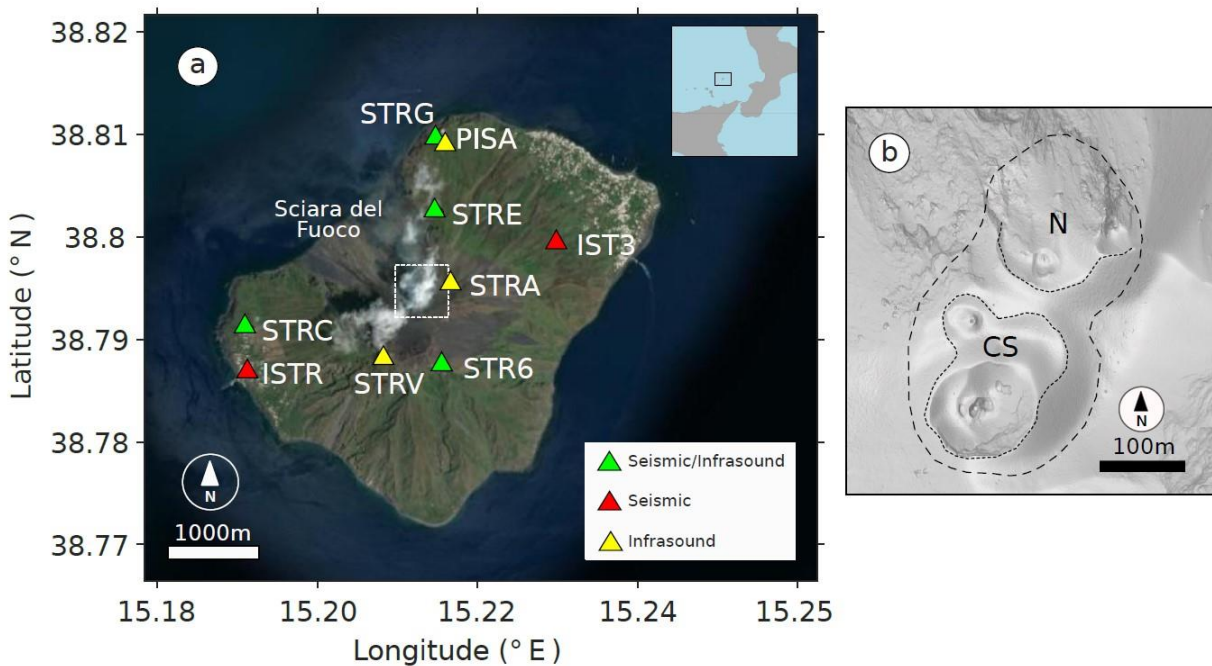


32 events, referred to as major explosions, which eject centimeter-to-meter-sized ballistic projectiles; at times, sustained explosive
33 activity is accompanied by partial collapses of the crater rim due to the instability of accumulated material, and increased
34 magmastic pressure within the conduit system (Gurioli et al., 2013; Di Traglia et al., 2024). Since 2019, major explosions at
35 Stromboli have occurred with a frequency of about 4-5 events per year ejecting pyroclastic material to heights over a hundred
36 meters, which can travel beyond the summit crater area and potentially affect tourist paths (Rosi et al., 2013; Gurioli et al.,
37 2013). In heightened states of activity, Stromboli may also experience paroxysms, that is highly energetic eruptions that
38 generate eruptive columns exceeding 4 km in height, ballistics of up to 2 m in diameter and significant collapse activity from
39 the summit crater areas (Fig. 1). Paroxysms can be accompanied by the emplacement of pyroclastic density currents (PDCs)
40 along the Sciara del Fuoco (SdF, Fig. 1a), which can enter the sea and travel up to 2 km from the shoreline with demonstrated
41 potential to trigger tsunamis (Rosi et al., 2006; Calvari et al., 2006; D'Auria et al., 2006; Ripepe and Lacanna, 2024). Although
42 paroxysms are less frequent than major explosions, with an average occurrence of just one every four years since 2003, they
43 are the most impactful hazard for the island of Stromboli (Rosi et al., 2013). A recent paroxysm on 3 July, 2019, resulted in a
44 fatality (Giudicepietro et al., 2020; Giordano and De Astis, 2020; Andronico et al., 2021).
45 Unrest and eruption at Stromboli generate a broad range of geophysical signals. Nucleation and coalescence of gas bubbles
46 into gas slugs (Sparks, 2003; Burton et al., 2007; Caricchi et al., 2024), and their ascent within the conduit generates
47 characteristic seismic and deformation signals (Marchetti et al., 2009); gas slug bursting at the top of the magma column
48 produces infrasound waves (Colò et al., 2010). Real-time detection and monitoring of these signals are crucial for risk
49 mitigation at Stromboli as, in the recent past, major explosions and paroxysms have frequently been anticipated by detectable
50 changes in geophysical signals between tens of seconds and minutes before their occurrence (Giudicepietro et al., 2020; Ripepe
51 et al., 2021a; Longo et al., 2024).
52 Except for the 2019 eruptive activity, the most intense in recent years, Stromboli's paroxysms are typically preceded by periods
53 of lava effusion, or a general increase in surface activity that lasts for several days (Ripepe et al., 2009; Valade et al., 2016).
54 Several studies have suggested that effusive eruptions may act as a trigger for paroxysmal explosions through a mechanism of
55 decompression of the volcano plumbing system, evidenced by a drop in magma levels within the conduit (Aiuppa et al., 2010;
56 Calvari et al., 2011; Ripepe et al., 2017). The most significant effusive event in terms of its volume occurred between December
57 2002 and July 2003 (Ripepe et al., 2017), which caused landslides, triggered a partial collapse of the SdF and culminated in a
58 paroxysm on 5 April, 2003; this was the first large-scale paroxysmal event on record since 1985 (Calvari and Nunnari, 2023).
59 However, it should also be noted that effusive eruptions are not necessarily followed by paroxysms. An example is the
60 November 2014 effusive eruption, which did not lead to paroxysmal activity (Rizzo et al., 2015). At the other end of the
61 spectrum lies the paroxysm of July 2019, for which no clear increase in activity prior to the main event was recorded. As
62 highlighted by Laiolo et al. (2022), thermal and gas flow levels had slightly increased but remained below "alert" thresholds.
63 Multi-parameter data are crucial to understand unrest at Stromboli and to detect transitions between low-to-moderate activity
64 and more explosive phases (Pistolesi et al., 2011; Andronico et al., 2021). Several conceptual models have been proposed
65 accounting for the ordinary seismic activity observed at Stromboli and other similar volcanoes (e.g., Chouet et al., 2008;



66 Suckale et al., 2016; Ripepe et al., 2021b). Petrological analyses of erupted products suggest the presence of a stratified conduit
67 at Stromboli, consisting of two types of magma (Bertagnini et al., 2003; Francalanci et al., 2004; Francalanci et al., 2005). The
68 upper conduit is thought to host highly porphyritic (HP) magma that is water-poor and rich in phenocrysts, and is erupted as
69 scoria during ordinary activity; on the other hand, magma in the lower conduit is gas-rich, low-porphyritic (LP), and typically
70 erupted as pumice alongside HP scoria and lithic blocks removed from conduit walls. Eruptive activity at Stromboli is inferred
71 to be controlled by the buoyant ascent and bursting of gas slugs (Sparks, 2003; Burton et al., 2007; Caricchi et al., 2024;
72 Aiuppa et al., 2010) from the top of the LP magma, rising through the more crystalline HP magma acting like a viscous fluid
73 or a rigid plug and controlling the final ascent and explosion of the slugs (Suckale et al., 2016). A recent model by (Caricchi
74 et al., 2024) shows that the instability of gas-rich and low-density foam layers at the base of the magma column could also
75 potentially trigger paroxysmal explosions at open conduit volcanoes.

76 In this study, we report on the most recent paroxysm at Stromboli, which occurred on 11 July, 2024, after a month of unrest at
77 the summit craters, as reported by the Istituto Nazionale di Geofisica e Vulcanologia (INGV) (INGV-OE, 2024). We analyze
78 the precursory geophysical activity leading up to the paroxysm based on seismic, infrasound and ground deformation data
79 gathered by the INGV monitoring network, complemented by observations conducted with an Unoccupied Aircraft System
80 (UAS) during the study period. The UAS imagery provides a valuable tool to interpret geophysical data and understand the
81 conditions leading up to the paroxysm on 11 July, offering a high-resolution reconstruction of the eruptive events and
82 associated morphological changes at the volcano. Unless, otherwise stated, all descriptions of surface activity in this
83 manuscript are from direct field observations by the authors during the study period.



85 **Figure 1: a) Map of monitoring network at Stromboli, showing the locations of seismo-acoustic, seismic, and infrasound sensors.**
86 **The inset shows the location of Stromboli volcano in Italy (MATLAB-Mapping Toolbox). b) Detail of the summit area of Stromboli,**
87 **corresponding to the white dash-line square in a), showing the summit crater areas.**

88 **2 Chronology of eruptive activity during 3-11, July, 2024**

89 The activity bulletins issued by INGV (see Data Availability), from May 24 until the early days of July, reported an increase
90 in surface activity at Stromboli, particularly from the North (N) crater area (Fig. 1b), characterized by continuous and intense
91 spattering, that is quasi-continuous emission of pyroclastic material through sequential, small-to-moderate, explosions ejecting
92 ballistics at heights of ~10-20 m above the vent (Harris and Ripepe, 2007; Giudicedipietro et al., 2021) (Fig. 2a). The average
93 frequency of explosions fluctuated between 13 (medium) and 16 (high) events/hour with spattering occasionally leading to
94 lava flows along the SdF (Fig. 1a). On June 23 and 28, lava flows began, following intense spattering from the N crater,
95 converging into a canyon-like structure created by previous PDC activity in October 2022 (Di Traglia et al., 2024). Sulfur
96 dioxide (SO₂) and carbon dioxide (CO₂) emissions remained at average levels, as did the carbon-to-sulfur (C/S) ratio (INGV-
97 OE, 2024).

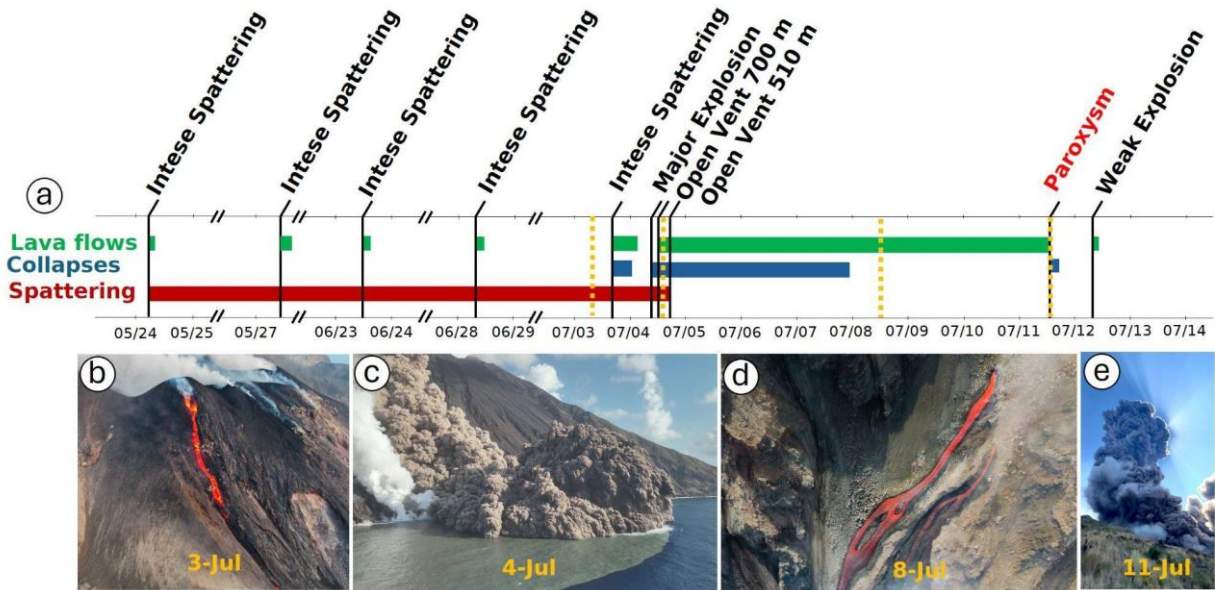
98 On 3 July, at 16:35 UTC, intense spattering was observed from a vent located within the N crater sector, leading to a sequence
99 of partial collapses of the N crater rim, which also remobilized material that had been erupted in the preceding days. These
100 collapses mostly consisted of cold material with a minor contribution of hot deposits. At 17:02 UTC, a lava flow began from
101 the same vent, accompanied by spattering and moderate explosions (Fig. 2b). The activity continued throughout the night, with
102 lava fronts moving down to an elevation of 550-600 m a.s.l..

103 On 4 July, at 12:16 UTC, a major explosion occurred from the N crater and, at 14:10 UTC, a new lava flow emerged at the
104 base of the N crater area at ~700 m a.s.l., advancing towards Bastimento and Filo di Fuoco, located along the northeast
105 boundary of SdF. After about one hour a second lava flow started at an elevation of ~580 m a.s.l., which reached the sea. At
106 16:15 UTC, another vent opened at ~510 m a.s.l., producing a third lava flow accompanied by PDCs that rapidly descended
107 the SdF into the sea (Fig. 2c). During the evening of 4 July, and throughout the following night, lava flow activity continued,
108 accompanied by occasional collapses of pyroclastic materials.

109 Between 5-6 July, 83 landslide events were observed, while effusive activity fluctuated and lava emission moved further
110 downslope originating from two new eruptive vents at ~485 m a.s.l. (Fig. 2d). The flow formed a delta at the shoreline and
111 steam plumes were observed caused by magma-seawater interaction. Explosive activity from the summit craters halted at the
112 beginning of the effusive phase.

113 On 11 July, at 12:08 UTC, a paroxysmal eruption occurred from the N crater area, producing an ash plume ~5 km high,
114 which dispersed towards the southwest (Fig. 2e). Shortly after, a pyroclastic flow rapidly advanced along the SdF, which
115 triggered a small-scale tsunami wave. The paroxysmal phase ended with a series of secondary and less intense PDCs.

116 In the following hours, effusive activity ceased, and no further explosions were observed, except for a minor event on 12 July,
117 at 08:28 UTC (Fig. 2a), which was followed by a small collapse event in the N crater area.



118

119 Figure 2: Timeline of the observed surface activity and key visual observations at Stromboli between late May and mid-July, 2024.
120 a) Timeline showing the chronology of activity, which marks periods of activity characterized by lava flows (green), collapses (blue),
121 and spattering (red). Significant events are labelled, such as intense spattering, a major explosion on 4, July, opening of new vents,
122 and the paroxysm on 11, July. b-e) Sequence of images gathered at the times indicated by the dashed yellow lines in a). From left to
123 right: spattering activity on 3, July, a PDC event reaching into the sea on 4, July, continued lava flow on 8, July, and the paroxysmal
124 explosion on 11, July (photo "e" courtesy of G. De Rosa - OGS).

125 3 Geophysical observations

126 In this study we use data recorded by the geophysical monitoring network deployed and maintained on Stromboli by INGV
127 (Fig. 2a). The network includes seismic (ISTR3, ISTR) and infrasound sensors (STRA, STRV), as well as seismo-acoustic
128 stations (STR6, STRC, STRE, STRG). An additional infrasound sensor, PISA (Gheri et al., 2024), was deployed on 4 July at
129 13:35 UTC, 35 minutes before the onset of the effusive activity.

130 3.1 Seismic characterization of unrest and eruptive events

131 Volcanic tremor is traditionally thought to reflect magma movement within the conduit (McNutt and Nishimura, 2008; Chouet
132 et al., 1997; Ripepe and Gordeev, 1999); at Stromboli, tremor is routinely monitored by means of the Root Mean Square (RMS)
133 of the continuous seismic signal in the 1-3 Hz frequency band (Giudicepietro et al., 2023). Figure 3a shows RMS values of the
134 order of $10-6 \text{ ms}^{-1}$ (recorded at the IST3 site), which correspond to tremor classified by INGV as high. A marked and short-
135 lived increase in seismic RMS was observed after the major explosion at 12:11 on 4 July (Fig. 3a). During this period, the
136 signal reached unprecedented levels, peaking at $10-4 \text{ m s}^{-1}$ at 17:00 UTC. Short-lived increases in RMS values were still noted

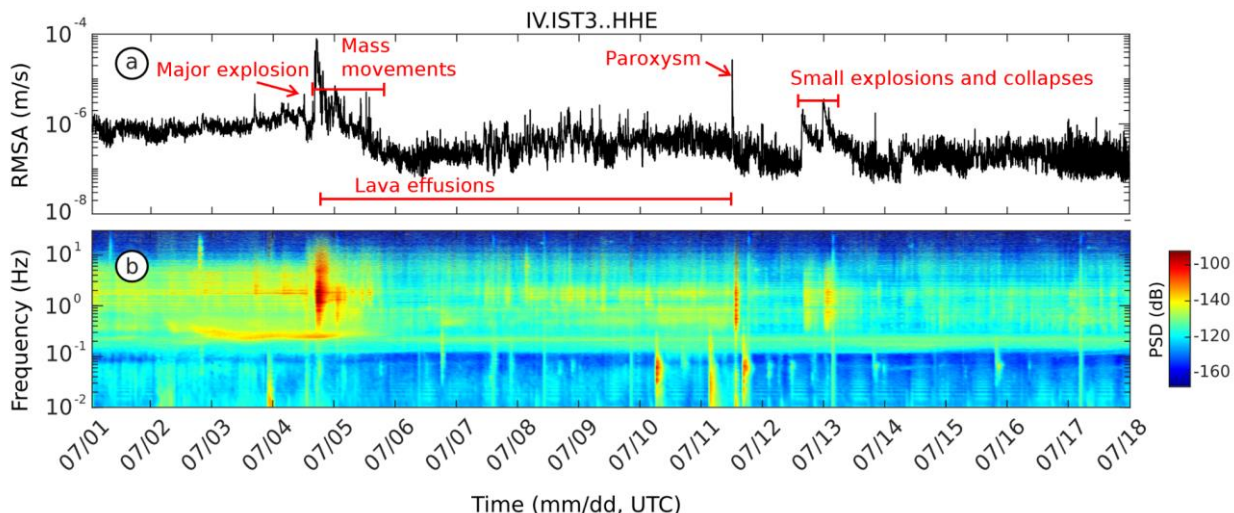


137 throughout 5 July, although the amplitudes exhibited an overall decline to values of the order of $10\text{-}7 \text{ m s}^{-1}$, lower than those
138 recorded at the beginning of July. In the following days (6-11 July), the tremor was marked by a series of short-duration peaks
139 during lava flow activity. This behavior changed again on 11 July, when the onset of paroxysmal activity coincided with a
140 new increase in RMS (Fig. 3a). After the paroxysm, the RMS decreased again with only sparse and brief intervals of increased
141 amplitudes between 12-13 July (Fig. 3a). From late on 13 July, onwards, the amplitude stabilized around $10\text{-}7 \text{ m s}^{-1}$, indicating
142 that volcanic activity had reduced and returned to background levels. Additional details of the signals recorded on 4-7 July,
143 are shown in the Supplementary Materials (Fig. 1S).

144 The spectrogram in Fig. 3b shows nearly continuous energy in the 2-3 Hz range, typically associated with tremor signals at
145 Stromboli (Ripepe et al., 1996). Energy levels in this band change throughout the pre-, syn-, and post-explosive activity
146 periods, reaching a maximum on 4 July following the major explosion. A pulsating phase was observed from 6-11 July, with
147 another peak during the paroxysm. Explosive activity between 4-11 July, exhibited a broader frequency range in the 0.5-15
148 Hz band. It is worth noting that the eruptive event on 4 July was preceded by a high-energy signal in the narrow frequency
149 band 0.2-0.3 Hz (Fig. 3b). We also observe that this very low-frequency signal was not recorded before the paroxysm on 11,
150 July. Finally, on July 10 at 05:09 UTC and on 11 July at 02:26 and 15:21 UTC, high-energy signals were observed around
151 0.05-0.08 Hz, exhibiting a dispersive spectrum typical of teleseismic events as reported by USGS (for further information, see:
152 <https://earthquake.usgs.gov/earthquakes/search/>).

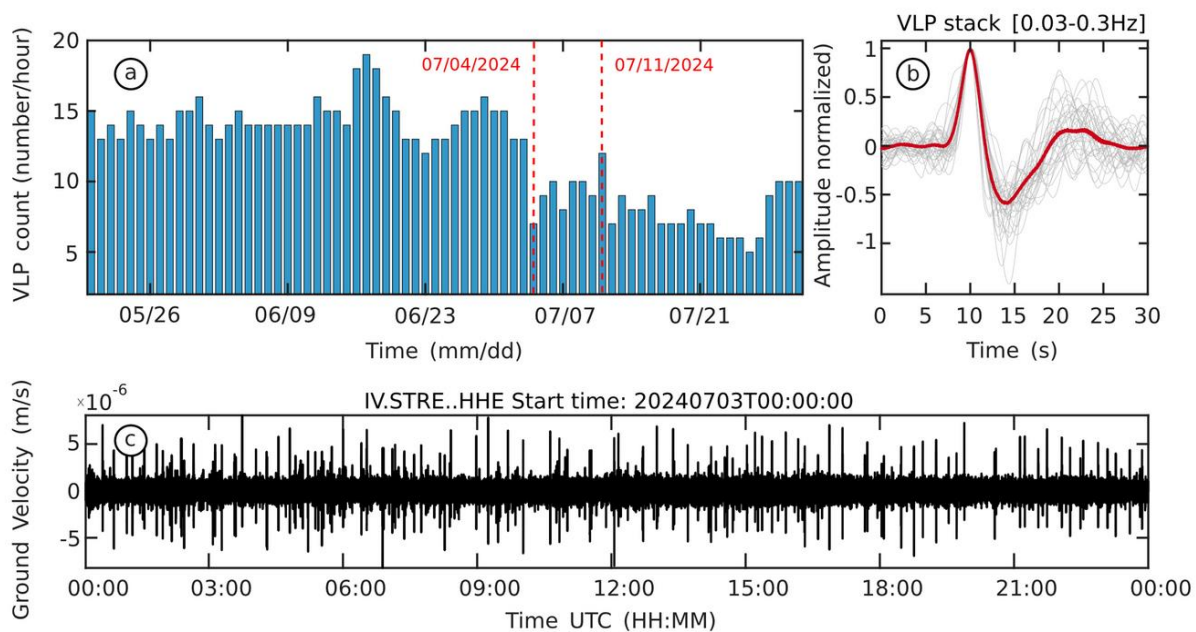
153 We have also analysed the occurrence of Very Long Period (VLP) earthquakes that have traditionally been associated with
154 pressure disturbances and the dynamics of gas-rich magma within fluid-filled structures (Chouet et al., 1997; Chouet et al.,
155 1999; Marchetti and Ripepe, 2005; Legrand and Perton, 2022), and one of the main tools used to monitor unrest at Stromboli.
156 An increase in the frequency of occurrence of these signals is typically a precursor to periods of elevated eruptive activity
157 (Ripepe et al 2009; Delle Donne et al., 2017). Figure 4a derived from information sourced from the INGV bulletins (INGV-
158 OE, 2024), provides an overview of the rates of VLP seismicity at Stromboli between the end of May and mid-July 2024, after
159 the 11 July paroxysm. From May until mid-June, VLP event rates remained stable, fluctuating around high values between 12
160 and 19 events/hour. A mean rate of \sim 13 events/hour is defined, at Stromboli, as “normal activity” (Ripepe et al., 2008) and it
161 suggests that an efficient degassing mechanism of the magma column is established (Ripepe et al., 2021b). A significant peak
162 is observed around mid-June, with the number of VLP events reaching a high of 19 events/hour on June 16. This peak is
163 followed by a slight decrease in event rates, although the number of events remained elevated compared to previous days.
164 Figure 4b shows the characteristic compression-decompression cycle of VLP events at Stromboli; this waveform represents
165 the normalized stack of all VLP events with maximum amplitude greater than $5 \times 10\text{-}6 \text{ m s}^{-1}$ at station STRE. Figure 4c shows
166 a 1-day filtered (0.03-3Hz) seismic record illustrating the occurrence of VLP events as recorded at station STRE, on the east
167 flank of SdF at 495 m of elevation (see Fig. 1).

168 Before the major explosion on 4 July, we observed a clear drop in the occurrence of VLP events (Fig. 4a) from 10-15 to 7-10
169 events/hour. The rates of VLP events remained stable until the 11 July paroxysm, peaking again at 12 events/hour on that day.
170 After the paroxysm, a further decrease in VLP rates was observed with hourly counts ranging from 6 to 10 events.



171

172 **Figure 3:** a) Seismic tremor or RMS calculated every minute using a moving time window of 5 minutes, within the volcanic tremor
 173 frequency band of Stromboli (1-3 Hz), from July 2 to 18. b) Spectrogram of the E-component from the IST3 seismic station for the
 174 same period.



175

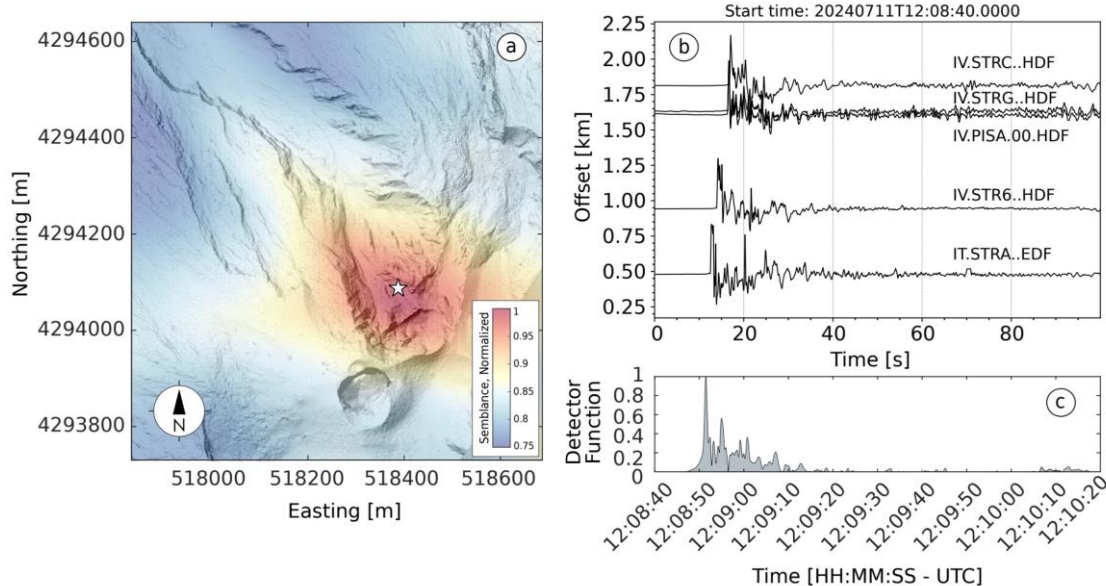
176 **Figure 4:** a) Hourly rates of VLP events from the INGV catalog. Vertical red dashed lines indicate the major explosion and paroxysm
 177 that occurred on 4 and 11, July, respectively. b) VLP waveform events ($>5 \times 10^{-6} \text{ m s}^{-1}$) recorded on 3, July, at station STRE
 178 normalized with respect to maximum amplitude (light grey). The red waveform represents the average of all high-amplitude
 179 waveforms. c) Continuous waveform recorded at station STRE (EW component) on 3, July 2024, filtered between 0.03-0.3 Hz.



180 3.2 Infrasound characterization of unrest and eruptive events

181 We have also analysed infrasound data recorded by the INGV acoustic monitoring network and an additional microphone
182 installed during the period of activity (Fig. 1). The infrasonic record before 4, July, shows a typical background of moderate
183 strombolian activity occasionally interspersed with larger explosions (see Fig. 2Sa). The major explosion on 4 July, generated
184 an infrasonic transient with a pressure of 5 Pa (Fig. 2Sb) at station STR6, from the CS crater area. Following this event, a
185 marked decrease in acoustic energy was observed until the 11, July paroxysmal event, which produced infrasonic waves with
186 a peak amplitude of 115 Pa at the STR6 site (approximately at ~750 m, see Fig.1a and Fig.2Sb).

187 We have used the infrasound records from all operating sensors of the INGV monitoring network on Stromboli and an
188 additional temporary microphone (Fig. 2) to locate the source of the paroxysmal eruption on 11, July 2024. We employed the
189 RTM-FDTD (Reverse Time Migration - Finite Difference Time Domain) method of Fee et al. (2021), which implements
190 waveform back-projection over a grid of candidate source locations. Travel-times between potential source locations and all
191 stations in the network are calculated via FDTD modeling (Kim and Lees, 2014; Fee et al., 2017; Diaz-Moreno et al., 2019)
192 to account for the effect of topography on the propagation of the acoustic wavefield. In the RTM-FDTD method, waveforms
193 are back-projected and a detector function (e.g., network stack, network semblance) is evaluated for each candidate source,
194 with the detector maximum corresponding to the most likely location. For FDTD calculations of travel-times we employed a
195 UAS-derived Digital Elevation Model (DEM) of the SdF and the summit craters (Civico et al., 2024) areas conducted on the
196 morning of 4 July with initial individual resolutions ranging between 20 and 50 cm/pixel. This DEM was merged with a
197 basemap elevation model (Civico et al., 2021) of the rest of the island, re-sampled, and parsed into a 5x5 m grid for the purpose
198 of FDTD modeling. For FDTD modeling, the source time function was approximated by a Blackman-Harris function with a
199 cutoff frequency of 5 Hz (high enough to include the dominant frequency of the explosion signals while still allowing time-
200 efficient computing) and the acoustic wavefield was propagated along the discretized topography using 15 grid points per
201 wavelength (Wang, 1996). We used a constant sound velocity of 330 m s⁻¹ (estimated from the signal move-out across the
202 network) and a stratified atmosphere model based on density and temperature data obtained from the Reanalysis v5 (ERA5)
203 dataset (see Data and Resources), produced by the European Centre for Medium-Range Weather Forecasts of the Copernicus
204 Climate Change Service. We used data corresponding to the ERA5 grid node closest to Stromboli, at 12:00 on 11, July 2024
205 (Coordinated Universal Time, UTC). The inferred source location for the paroxysmal explosion on 11, July 2024, along with
206 a record section of the infrasound waveforms used and the detector function, are shown in Fig. 5. The location identifies a
207 source located approximately 50m below the rim of the N crater (Fig. 5a) at an elevation of ~685 m. The estimated origin time
208 for the event is 12:08:52 UTC.



209

210 **Figure 5: Infrasound location of the 11 July, 2024 paroxysmal event using the RTM-FDTD method (see manuscript for details; DEM**
211 **of July 14, 2024 from Civico et al. (2024). a) Map-view of network semblance maximum around the Stromboli crater region. RTM-**
212 **FDTD semblance location is indicated by a white star; b) record section of the filtered infrasound waveforms (bandpass filter 0.01-**
213 **15Hz) used for locating the event. The offset corresponds to source-station distance; c) Normalized network detector function (i.e.,**
214 **maximum network semblance amplitude over time).**

215 3.3 Deformation of unrest and eruptive events

216 Ground tilt at Stromboli has been frequently inferred to reflect processes like slug coalescence, slug ascent, and conduit
217 emptying (Marchetti et al., 2009; Genco and Ripepe, 2010; Bonaccorso, 1998). Over the last decade, tilt has become central
218 to real-time monitoring and eruption early warning at Stromboli. Ripepe et al. (2021a), for example, demonstrated the scale
219 invariance of tilt at Stromboli, that is all explosions, regardless of their intensity, follow the same ground inflation-deflation
220 pattern. A significant tilt was reported on 4 July (INGV-OE, 2024). The major explosion at 12:00 UTC was accompanied by
221 a characteristic inflation-deflation pattern (Longo et al., 2024), followed by a pronounced deflation trend that began at 16:20
222 UTC and continued until 19:50 UTC (INGV-OE, 2024).

223

224 For the paroxysm on 11, July 2024 fig. 5 shows the seismic-derived tilt, reconstructed from the EW horizontal component
225 record at station STRE Aoyama et al. (2008), Genco and Ripepe (2010), and De Angelis and Bodin (2012). Slow inflation is
226 observed, starting approximately 600 seconds before the explosion (Fig. 5b); the seismic-derived tilt sharply accelerates
227 approximately 1 minute before reaching its peak of 1.5 μ rad at the onset of the explosion, followed by rapid deflation. This
228 pattern is consistent with previous observations of tilt at Stromboli before paroxysms and major explosions (e.g. Genco and
229 Ripepe (2010); Ripepe et al. (2021a)). We note that this tilt signal is derived from an individual seismic record, of an instrument



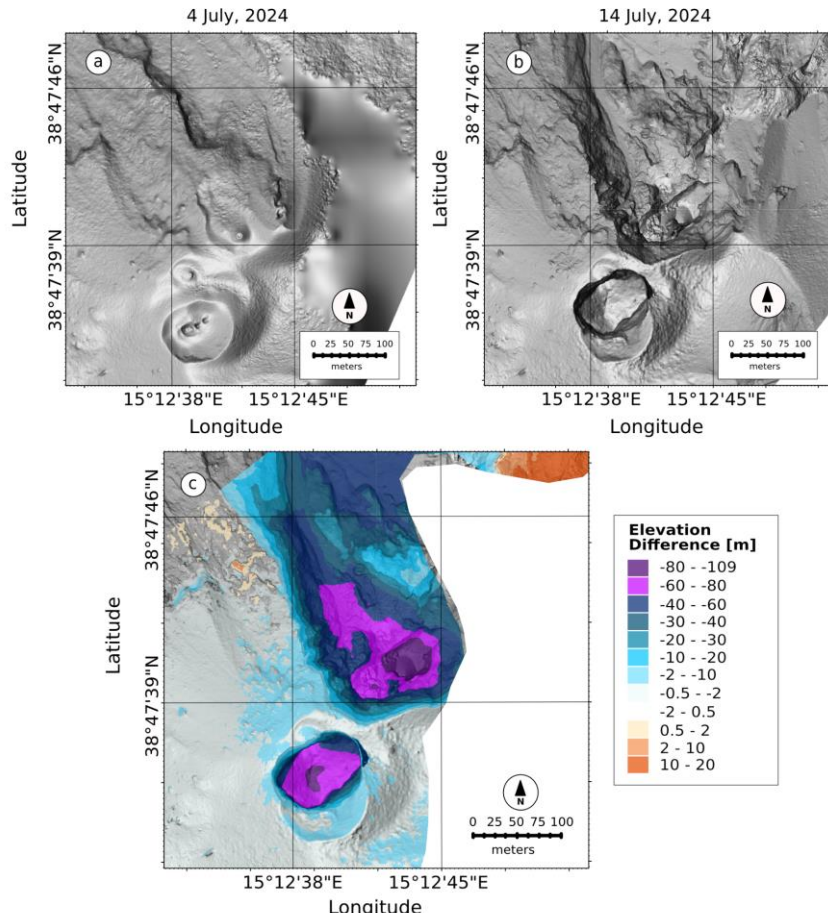
230 that is not likely oriented in the direction radial to the source; for this reason, we will focus on the interpretation of the
231 deformation trend, and will not use the measured tilt amplitude for modelling purposes.

232 **4 Discussion**

233 In this manuscript we have presented geophysical data recorded between early and mid-July 2024 at Stromboli; the period of
234 unrest included a major explosion on 4 July, significant collapse activity in the N summit crater area, emplacement of lava
235 flows, and a paroxysmal event on 11 July. Surface activity at Stromboli intensified late in May with a marked increase in the
236 occurrence of Strombolian explosions, the onset of effusive activity from SdF, and increasing volcanic tremor. Early in July,
237 we observed a steady increase in volcanic tremor reaching unprecedented amplitudes on 4 July, (see Fig. 3a and Fig. 1S).
238 Volcanic tremor at Stromboli has typically been linked to the coalescence of gas bubbles from layers of smaller bubbles and
239 their ascent along the shallower conduit (McNutt et al., 2008; Chouet et al., 1997; Ripepe et al., 1999), suggesting that
240 variations in tremor intensity are controlled by changes in gas flow within the conduit. It has been frequently speculated that
241 an increase in volcanic tremor reflects an increase in the volume of gas within the magma (Ripepe et al., 1996), which in turn
242 is linked to a higher occurrence of explosions at the top of the magma column. Field observations of increasing spattering in
243 early July (Fig. 1) support a model of increased surface activity linked to the ascent of gas-rich magma within the shallow
244 conduit. The high rates of VLP events observed during the same period further support the hypothesis of gas-rich magma
245 migration within the shallow plumbing system. These events are traditionally associated with the rapid expansion of gas slugs
246 rising through the liquid melt in the shallow conduit (Chouet et al., 2003; James et al., 2006); more recently (Ripepe et al.,
247 2021) suggested that VLP waveforms at Stromboli are generated at the top of the magma column, mainly after the onset of
248 Strombolian explosions; they showed that the occurrence of VLP event can be linked to explosive magma decompression in
249 the uppermost ~ 250 m of the conduit. The recorded VLP events showed similar waveforms (Fig. 4b) suggesting a stable source
250 mechanism and location; locations in the shallow parts of the conduit can be linked to magma accumulation at a shallow depth,
251 close to the surface. While the number of VLP events did not show any significant variation before the major explosion on 4
252 July, volcanic tremor increased slowly but steadily (Fig. 3a). Coinciding with strong ground deflation after the major explosion
253 (INGV-OE, 2024), volcanic tremor reached an unprecedented peak amplitude of ~8 x 10⁻⁵ m s⁻¹ at ~17:00 UTC associated
254 with the opening of a new effusive vent at ~ 510 m elevation within SdF (Fig. 2a) and the occurrence of numerous mass
255 wasting events linked to collapse activity within the lower N crater area and upper section of SdF. We suggest that these signals
256 reflect the emptying of the shallowest parts of the conduit system and the overall lowering of the magma level within the
257 shallow volcano plumbing reflected in the opening of new effusive vents at progressively lower elevations. The transition
258 between explosive and effusive regimes was also marked by a clear decrease in the occurrence of VLP events (Fig. 4), and a
259 migration of their source deeper within the conduit (Ripepe et al., 2015). This contrasts with the flank eruptions of 2007 and
260 2014 (Ripepe et al., 2009; Ripepe et al., 2015) when VLP rates remained high during effusion; in July 2024 it appears that
261 effusion reduced the overall explosivity, rather than recalling fresh magma from depth. The new effusive regime, indeed, was



262 characterized by a substantial lack of Strombolian explosive activity at the surface between 4-11 July, as observed in the field
263 by our research team. The quasi-continuous collapse activity, observed from 13:00 UTC on 4, July, appeared to be linked to
264 instabilities in the crater area around newly created vents; this instability persisted in the following days, with the number of
265 events peaking on July 5 (83 recorded occurrences recorded in a single day (INGV-OE, 2024). The collapse activity recorded
266 along the N crater rim, adjacent to the SdF, resulted in significant changes to the morphology of this sector of the volcanic
267 edifice (Fig. 6).
268 During the study period, we also collected UAS data and compiled very high-resolution repeat DEMs (0.2-0.5 m/pixel), which
269 allowed quantifying topographical changes via DEM differencing. The difference between DEMs on 4, July, (morning) and
270 July 14 is shown in Fig. 7c. The data processing methodology follows the procedures described in Civico et al. (2022, 2024).
271 The most notable morphological variations were observed in the afternoon of 4 July, while the paroxysm on 11 July did not
272 lead to significant changes.
273 The summit craters were affected by loss of material due to the opening of two eruptive vents at approximately 700 and 500
274 m a.s.l.. While the CS crater sector showed a roughly circular-shape crater floor deepening of about 84 m, the N sector was
275 affected by the complete dismantling of its northern rim and external slope, marking the deepest morphological change
276 occurred at the summit craters in the last decades, with a maximum difference in altitude of 109 m. The total volume loss
277 recorded in the summit craters sector was estimated at 3.3 Mm³ (Civico et al., 2024).



278

279 **Figure 6: Multidirectional hillshades of Stromboli's crater area: a) 4, July 2024 (Civico et al., 2024c), b) July 14, 2024 (Civico et al.,
280 2024), c) map of elevation difference (Dem of Differences) highlighting morphological changes occurred between 4 and 14 July, 2024.
281 Purple areas indicate material loss, whereas orange areas indicate material gain.**

282 Unlike the summit craters, the subaerial portion of the SdF slope was affected by both accumulation and erosion processes.
283 Here, the main loss of material (2.74 Mm³; Civico et al., 2024a) was localized along the canyon formed in October 2022 (Di
284 Traglia et al., 2024), which has widened and deepened during the July 2024 eruption. Accumulation processes instead were
285 mainly due to PDC and lava flow deposits, localized in the northeastern sector of the slope. The maximum accumulation of
286 lavas occurred at the new lava delta (maximum difference in altitude of 45 m), located in the center of the SdF shoreline.
287 The effusive regime ended with the occurrence of the paroxysmal explosion on 11, July. The explosion generated an infrasonic
288 pressure of 115 Pa at station STR6 with an associated VLP amplitude reaching 5.8×10^{-5} m s⁻¹ (see Fig. 3S). An ash plume
289 reached a height of 5 km above the vent, and pyroclastic flows moved down the SdF. After that, volcanic activity reduced its
290 intensity, showing low levels of tremor and VLP events although the tremor increased again on 12, July, associated with a
291 small lava flow.



292 The eruptive crisis of July 2024, culminating in the paroxysm, is consistent with previous eruptions at Stromboli, such as those
293 in April 2003, March 2007, and July-August 2019. The data discussed above can be used to inform a conceptual model of the
294 entire sequence of processes responsible for the observed surface and eruptive activity, within the framework of previous
295 studies (e.g., James et al., 2006; Chouet et al., 2008; Del Bello et al., 2012; Suckale et al., 2015; McKee et al., 2022).
296 The spattering activity, observed at the start of our study period, represents an intensified form of puffing. Spattering activity
297 results from the quasi-continuous bursting of small gas pockets within a bubbly flow regime, which generates pyroclasts
298 fragments (Rosi et al., 2013). This activity typically marks the initial stages of unrest and eruption at Stromboli, where gas-
299 rich magma is being actively degassed through continuous explosive bursts (Del Bello et al., 2012). At the more explosive end
300 of the spectrum of Strombolian activity major explosions and paroxysms are often explained invoking the "slug model" (James
301 et al., 2006; Chouet et al., 2008; Del Bello et al., 2012). In this model, gas bubbles (slugs) form deeper in the magma column
302 and gradually coalesce as they rise through the conduit due to an increase of the magma viscosity. As gas slugs ascend, they
303 expand due to decreasing pressure and eventually reach the surface. When they burst at the top of the magma column, they
304 release gas explosively, fragmenting the magma and producing pyroclasts and feeding ash plumes of varying sizes. After the
305 major explosion on 4 July, an effusive regime was established, characterized by lava flows, during which more degassed
306 magma was erupted. Following the initial explosive activity driven by gas slugs, we infer that the transition to effusive regime
307 is controlled by depressurization of the shallow plumbing system similar to Ripepe et al. (2017). The depressurization of the
308 system caused by the initial explosive activity allowed magma to flow, and reach the surface forming lava flows, without
309 further explosive activity. As the shallow volcanic conduit progressively emptied it leads to structural instability, causing
310 collapses and landslides along the SdF.
311 According to Ripepe et al. (2017), the emptying of the conduit creates a vacuum effect that draws more gas-rich magma from
312 deeper within the system. As volatile-rich magma rises and encounters lower pressures, it can lead to explosive eruptions,
313 resulting in a paroxysmal event. The dynamics of the 11, July paroxysmal explosion displayed similar trends across seismic,
314 acoustic, and deformation parameters compared to the others (Genco and Ripepe, 2010; Ripepe et al., 2021a). This consistency
315 further validates the established models of Strombolian activity, where the largest explosions and energetic events, such as
316 paroxysms, are driven by the same source mechanism. The scale-invariant conduit dynamics of ground deformation
317 demonstrate that inflation amplitude and duration scale directly with the magnitude of the explosion (Ripepe et al., 2021a).
318 Ground deformation observed on 11, July (Fig. 5) follows the same exponential inflation pattern as seen in previous paroxysms
319 (Ripepe et al., 2021a). This behavior is typically explained by bubble dynamics, where the pressure on the conduit walls
320 increases due to the rapid volumetric expansion of gas in highly vesiculated magma. As gas rises and expands, moreover, it
321 pushes the magma column toward the surface, often leading to precursory lava emissions from the vent. Ground deformation
322 is likely caused by a combination of increasing magma static pressure and the pressurization of degassed magma at the top of
323 the column, driven by the exponential growth of gas. When the pressure applied by the gas-rich magma exceeds the tensile
324 strength of the viscous magma plug, fragmentation occurs, resulting in the explosive release of gas and pyroclastic material
325 (e.g. paroxysm). Another possible mechanism, proposed by Suckale et al. (2016) and McKee et al., (2022) suggests that the



326 explosion is triggered by the rapid expansion and release of gas when a partial rupture occurs in the plug at the top of the
327 magma column.

328 **5 Conclusion**

329 The eruptive activity at Stromboli starting from 4, July, and culminating on 11, July 2024, with the paroxysm, provides a
330 comprehensive case study of explosive volcanism at open-conduit volcanoes, thus offering additional insights and proofs for
331 already existing source models.

332 The July 2024 paroxysm is preceded by a prolonged phase of heightened activity, characterized by increased volcanic tremor
333 and VLP events. The high seismicity, combined with observed crater rim collapses and lava flows, suggests a progressive
334 destabilization of the volcanic edifice. In particular, the major explosion on 4, July, and the subsequent paroxysm on 11, July
335 highlight the role of magma gas dynamics, where increased gas volumes and pressure led to significant eruptive events.

336 Seismic analysis reveals that the volcanic tremor intensity is linked to gas-rich magma movement, reaching in this eruptive
337 sequence unprecedented values at Stromboli. However, the variability in VLP events indicates that, while useful for monitoring
338 overall volcano unrest, these signals alone may not serve as reliable precursors for major explosive events. Instead, the
339 combined analysis of different geophysical parameters, including ground deformation, proved crucial for early warning and
340 forecasting as previously suggested by Ripepe et al. (2021a).

341 Ground deformation patterns, specifically the inflation-deflation cycle observed before explosions, align with previous studies,
342 confirming that such patterns reflect the occurrence of imminent explosions regardless of their magnitude. The exponential
343 inflation observed before the paroxysm, caused by gas expansion and the rise of slugs within the magma column, is the same
344 as in other paroxysmal events at Stromboli, supporting the already proposed source mechanism models for explosive events.

345 Through UAS data, Civico et al. (2024) were able to estimate a total volume loss of about 6.0 Mm³ involved after the
346 gravitational mass collapses occurred on 4 and 11 July. The partial collapses generated a reshaping of the summit craters area
347 as well as a deepening 2022 canyon along SdF, thus increasing the flank instability.

348 In conclusion, our results demonstrate how geophysical, visual observation and UAS-derived topographic data could offer
349 valuable insights for tracking the volcanic explosive phenomena as well as the partial collapses of the summit craters due to
350 the flank instability. This multiparametric monitoring approach could lead to significant advancements in reducing volcanic
351 hazards at Stromboli.

352 **Data availability**

353 The seismic waveform data from all the stations are part of INGV seismic network. The data are publicly available at EIDA
354 Italia (<https://eida.ingv.it/>). The infrasound data are available upon request from the INGV- Osservatorio Vesuviano. The
355 infrasonic collected from PISA station are available at <https://doi.org/10.5281/zenodo.14245572>.



356 **Author contribution**

357 L.Z., S.D.A. and P.S. wrote the proposals that funded installation and maintenance of the infrasound array and UAS, designed
358 the field experiment, and financially supported this publication. L.Z. and S.D.A. tested the infrasonic equipment, organized
359 fieldwork and participated in the original design of the experiment. L.Z., S.D.A., R.C., T.R. contributed to assembling the final
360 multiparametric dataset and tested its quality and retrieval. L.Z., R.C. and T.R. installed and maintained the equipment during
361 the field acquisition. L.Z., S.D.A. and D.G. performed analyses of infrasound data, seismic and tilt data, and prepared all
362 figures. R.C. and T.R. analysed the UAS images. L.Z., D.G. and S.D.A. jointly wrote the initial draft of the manuscript and all
363 authors contributed to review and edit the final version.

364 **Competing interests**

365 The authors declare that they have no conflict of interest.

366 **Acknowledgements**

367 INGV Project 'Pianeta Dinamico (Dynamic Planet) - Working Earth': Geosciences For The Understanding The Dynamics Of
368 The Earth And The Consequent Natural Risks - "Dynamo - DYNAmics of eruptive phenoMena at basaltic vOlcanoes"
369 (<https://progetti.ingv.it/it/pian-din/dynamo#project-info>).
370 INGV Departmental Strategic Project "UNO - UNderstanding the Ordinary to forecast the extraordinary: An integrated
371 approach for studying and interpreting the explosive activity at Stromboli volcano" (<https://progetti.ingv.it/it/uno-stromboli>).
372 L.Z., D.G., S.D.A., R.C., T. R. and P.G. are supported by the grant "Progetto INGV Pianeta Dinamico" -Sub-project
373 VT_DYNAMO 2023- code CUP D53J19000170001 - funded by Italian Ministry MIUR ("Fondo Finalizzato al rilancio degli
374 investimenti delle amministrazioni centrali dello Stato e allo sviluppo del Paese", legge 145/2018).
375 We are indebted to all the INGV colleagues who have contributed to the monitoring efforts on Stromboli during July 2024 and
376 the ones involved in the surveillance and network maintenance activities, to Maria Zagari (Italian Civil Aviation Authority -
377 ENAC) for her help in issuing new NOTAMs during the emergency, and to Giuseppe De Rosa, Istituto Nazionale di
378 Oceanografia e di Geofisica Sperimentale (OGS) for providing the photo of the 11, July paroxysm in Fig. 1.
379 The contents of this article represent the authors' ideas and do not necessarily correspond to the official opinion and policies
380 of the Dipartimento della Protezione Civile - Presidenza del Consiglio dei Ministri.e UAS images. We are grateful to the
381 "Gruppo monitoring dell'Osservatorio Vesuviano" of INGV, Osservatorio Vesuviano (Italy), for their support in the data
382 management.



383 **Financial support**

384 This work was supported by the grant "Progetto INGV Pianeta Dinamico" -Sub-project VT_DYNAMO 2023- code CUP
385 D53J19000170001 - funded by Italian Ministry MIUR ("Fondo Finalizzato al rilancio degli investimenti delle amministrazioni
386 centrali dello Stato e allo sviluppo del Paese", legge 145/2018) and by NGV Departmental Strategic Project "UNO -
387 Understanding the Ordinary to forecast the extraordinary: An integrated approach for studying and interpreting the explosive
388 activity at Stromboli volcano".

389 **References**

390 Aiuppa, A., Burton, M., Caltabiano, T., Giudice, G., Guerrieri, S., Liuzzo, M., and Salerno, G.: Unusually large magmatic
391 CO₂ gas emissions prior to a basaltic paroxysm, *Geophys. Res. Lett.*, 37, <https://doi.org/10.1029/2010GL044997>, 2010.

392 Andronico, D., Del Bello, E., D'Oriano, C., Landi, P., Pardini, F., Scarlato, P., and Valentini, F.: Uncovering the eruptive
393 patterns of the 2019 double paroxysm eruption crisis of Stromboli volcano, *Nat. Commun.*, 12, <https://doi.org/10.1038/s41467-021-23349-4>, 2021.

395 Bertagnini, A., Métrich, N., Landi, P., and Rosi, M.: Stromboli volcano (Aeolian Archipelago, Italy): An open window on the
396 deep-feeding system of a steady state basaltic volcano, *J. Geophys. Res. Solid Earth*, 108,
397 <https://doi.org/10.1029/2002JB002146>, 2003.

398 Bonaccorso, A.: Evidence of a dyke-sheet intrusion at Stromboli Volcano inferred through continuous tilt, *Geophys. Res. Lett.*,
399 25, <https://doi.org/10.1029/98GL00766>, 1998.

400 Burton, M., Allard, P., Murè, F., and La Spina, A.: Magmatic gas composition reveals the source depth of slug-driven
401 Strombolian explosive activity, *Science*, 317, <https://doi.org/10.1126/science.1141900>, 2007.

402 Calvari, S., Spampinato, L., and Lodato, L.: The 5 April 2003 vulcanian paroxysmal explosion at Stromboli volcano (Italy)
403 from field observations and thermal data, *J. Volcanol. Geotherm. Res.*, 149, <https://doi.org/10.1016/j.jvolgeores.2005.09.008>,
404 2006.

405 Calvari, S., Spampinato, L., Bonaccorso, A., Oppenheimer, C., Rivalta, E., and Boschi, E.: Lava effusion—A slow fuse for
406 paroxysms at Stromboli volcano? *Earth Planet. Sci. Lett.*, <https://doi.org/10.1016/j.epsl.2011.03.005>, 2011.

407 Calvari, S., and Nunnari, G.: Statistical insights on the eruptive activity at Stromboli volcano (Italy) recorded from 1879 to
408 2023, *Remote Sensing*, 15, <https://doi.org/10.3390/rs15174298>, 2023.

409 Caricchi, L., Montagna, C. P., Aiuppa, A., Lages, J., Tamburello, G., and Papale, P.: CO₂ flushing triggers paroxysmal
410 eruptions at open conduit basaltic volcanoes, *J. Geophys. Res.: Solid Earth*, 129, <https://doi.org/10.1029/2023JB02561>, 2024.

411 Chouet, B., Saccorotti, G., Martini, M., Dawson, P., De Luca, G., Milana, G., and Scarpa, R.: Source and path effects in the
412 wave fields of tremor and explosions at Stromboli Volcano, Italy, *J. Geophys. Res.: Solid Earth*, 102,
413 <https://doi.org/10.1029/96JB03395>, 1997.



414 Chouet, B., Dawson, P., Ohminato, T., Martini, M., Saccorotti, G., Giudicepietro, F., De Luca, G., Milana, G., and Scarpa, R.:
415 Source mechanisms of explosions at Stromboli Volcano, Italy, determined from moment-tensor inversions of very-long-period
416 data, *J. Geophys. Res.: Solid Earth*, 108, <https://doi.org/10.1029/2002JB001919>, 2003.

417 Chouet, B., Dawson, P., and Martini, M.: Shallow-conduit dynamics at Stromboli Volcano, Italy, imaged from waveform
418 inversions, *Geol. Soc. London, Special Publications*, 307, <https://doi.org/10.1144/SP307.5>, 2008.

419 Colò, L., Ripepe, M., Baker, D. R., and Polacci, M.: Magma vesiculation and infrasonic activity at Stromboli open conduit
420 volcano, *Earth Planet. Sci. Lett.*, 292, <https://doi.org/10.1016/j.epsl.2010.01.041>, 2010.

421 Civico, R., Ricci, T., Scarlato, P., Andronico, D., Cantarero, M., Carr, B. B., De Beni, E., Del Bello, E., Johnson, J. B.,
422 Kueppers, U., Pizzimenti, L., Schmid, M., Strehlow, K., and Taddeucci, J.: Unoccupied Aircraft Systems (UASs) Reveal the
423 Morphological Changes at Stromboli Volcano (Italy) before, between, and after the 3 July and 28 August 2019 Paroxysmal
424 Eruptions, *Remote Sensing*, 13, <https://doi.org/10.3390/rs13010141>, 2021.

425 Civico, R., Ricci, T., Cecili, A., and Scarlato, P.: High-resolution topography reveals morphological changes of Stromboli
426 volcano following the July 2024 eruption, *Sci. Data*, 11, 1219, <https://doi.org/10.1038/s41597-024-04098-y>, 2024.

427 D'Auria, L., Giudicepietro, F., Martini, M., and Peluso, R.: Seismological insight into the kinematics of the 5 April 2003
428 vulcanian explosion at Stromboli volcano (southern Italy), *Geophys. Res. Lett.*, 33, <https://doi.org/10.1029/2005GL025502>,
429 2006.

430 De Angelis, S., and Bodin, P.: Watching the Wind: Seismic Data Contamination at Long Periods due to Atmospheric Pressure-
431 Field-Induced Tilting, *Bull. Seismol. Soc. Am.*, 102, <https://doi.org/10.1785/0120110245>, 2012.

432 Del Bello, E., Llewellyn, E. W., Taddeucci, J., Scarlato, P., and Lane, S. J.: An analytical model for gas overpressure in slug-
433 driven explosions: Insights into Strombolian volcanic eruptions, *J. Geophys. Res.: Solid Earth*, 117(B2),
434 <https://doi.org/10.1029/2011JB008747>, 2012.

435 Diaz-Moreno, A., Iezzi, A. M., Lamb, O. D., Fee, D., Kim, K., Zuccarello, L., and De Angelis, S.: Volume Flow Rate
436 Estimation for Small Explosions at Mt. Etna, Italy, From Acoustic Waveform Inversion, *Geophys. Res. Lett.*, 46,
437 <https://doi.org/10.1029/2019GL084159>, 2019.

438 Di Traglia, F., Berardino, P., Borselli, L., Calabria, P., Calvari, S., Casalbore, D., et al.: Generation of deposit-derived
439 pyroclastic density currents by repeated crater rim failures at Stromboli Volcano (Italy), *Bull. Volcanol.*, 86,
440 <https://doi.org/10.1007/s00445-024-01516-0>, 2024.

441 Delle Donne, D., Tamburello, G., Aiuppa, A., Bitetto, M., Lacanna, G., D'Aleo, R., and Ripepe, M.: Exploring the explosive-
442 effusive transition using permanent ultraviolet cameras, *J. Geophys. Res.: Solid Earth*, 122(6), 4377–4394,
443 <https://doi.org/10.1002/2017JB014027>, 2017.

444 European Centre for Medium-Range Weather Forecasts (ECMWF), ECMWF Reanalysis v5. Available at:
445 <https://www.ecmwf.int/en/forecasts/dataset/ecmwf-reanalysis-v5>. Access date: 21 July 2024.



446 Fee, D., Izbekov, P., Kim, K., Yokoo, A., Lopez, T., Prata, F., Kazahaya, R., Nakamichi, H., and Iguchi, M.: Eruption mass
447 estimation using infrasound waveform inversion and ash and gas measurements: Evaluation at Sakurajima Volcano, Japan,
448 *Earth Planet. Sci. Lett.*, 480, <https://doi.org/10.1016/j.epsl.2017.09.043>, 2017.

449 Fee, D., Toney, L., Kim, K., Sanderson, R. W., Iezzi, A. M., Matoza, R. S., De Angelis, S., Jolly, A. D., Lyons, J. J., and
450 Haney, M. M.: Local Explosion Detection and Infrasound Localization by Reverse Time Migration Using 3-D Finite-
451 Difference Wave Propagation, *Front. Earth Sci.*, 9, <https://doi.org/10.3389/feart.2021.640202>, 2021.

452 Francalanci, L., Tommasini, S., and Conticelli, S.: The volcanic activity of Stromboli in the 1906–1998 AD period:
453 mineralogical, geochemical and isotope data relevant to the understanding of the plumbing system, *J. Volcanol. Geotherm.*
454 *Res.*, 131, [https://doi.org/10.1016/S0377-0273\(03\)00364-1](https://doi.org/10.1016/S0377-0273(03)00364-1), 2004.

455 Francalanci, L., Davies, G. R., Lustenhouwer, W., Tommasini, S., Mason, P. R. D., and Conticelli, S.: Intra-Grain Sr Isotope
456 Evidence for Crystal Recycling and Multiple Magma Reservoirs in the Recent Activity of Stromboli Volcano, Southern Italy,
457 *J. Petrol.*, 46, <https://doi.org/10.1093/petrology/egi062>, 2005.

458 Genco, R., and Ripepe, M.: Inflation-deflation cycles revealed by tilt and seismic records at Stromboli volcano, *Geophys. Res.*
459 *Lett.*, 37, <https://doi.org/10.1029/2009GL042925>, 2010.

460 Giordano, G., and De Astis, G.: The summer 2019 basaltic Vulcanian eruptions (paroxysms) of Stromboli, *Bull. Volcanol.*,
461 83, <https://doi.org/10.1007/s00445-020-01403-0>, 2020.

462 Giudicepietro, F., Calvari, S., De Cesare, W., Di Lieto, B., Di Traglia, F., Esposito, A. M., Orazi, M., Romano, P., Tramelli,
463 A., Nolesini, T., Casagli, N., Calabria, P., and Macedonio, G.: Seismic and thermal precursors of crater collapses and overflows
464 at Stromboli volcano, *Sci. Rep.*, 13, <https://doi.org/10.1038/s41598-023-30198-9>, 2023.

465 Giudicepietro, F., López, C., Macedonio, G., Alparone, S., Bianco, F., Calvari, S., ... and Tramelli, A.: Geophysical precursors
466 of the July-August 2019 paroxysmal eruptive phase and their implications for Stromboli volcano (Italy) monitoring, *Sci. Rep.*,
467 10, 10296, <https://doi.org/10.1038/s41598-020-67160-w>, 2020.

468 Gheri, D., Zuccarello, L., De Angelis, S., Ricci, T., and Civico, R.: Infrasonic Data from the July 4–11, 2024 Paroxysm of
469 Stromboli Volcano [Data set]. Zenodo. <https://doi.org/10.5281/zenodo.14245572>, 2024.

470 Gurioli, L., Harris, A. J. L., Colò, L., Bernard, J., Favalli, M., Ripepe, M., and Andronico, D.: Classification, landing
471 distribution, and associated flight parameters for a bomb field emplaced during a single major explosion at Stromboli, Italy,
472 *Geology*, 41, <https://doi.org/10.1130/G33576.1>, 2013.

473 Harris, A., and Ripepe, M.: Temperature and dynamics of degassing at Stromboli, *J. Geophys. Res.: Solid Earth*, 112(B3),
474 <https://doi.org/10.1029/2006JB004393>, 2007.

475 INGV Bulletin of 25/06/2024: <https://www.ct.ingv.it/index.php/monitoraggio-e-sorveglianza/prodotti-del-monitoraggio/bollettini-settimanali-multidisciplinari/914-bollettino-Settimanale-sul-monitoraggio-vulcanico-geochimico-e-sismico-del-vulcano-Stromboli-del-2024-06-25/file>, last access: 19 August 2024.



478 INGV Bulletin of 02/07/2024: <https://www.ct.ingv.it/index.php/monitoraggio-e-sorveglianza/prodotti-del-monitoraggio/bollettini-settimanali-multidisciplinari/915-bollettino-Settimanale-sul-monitoraggio-vulcanico-geochimico-e-sismico-del-vulcano-Stromboli-del-2024-07-02/file>, last access: 19 August 2024.

481 INGV Bulletin of 09/07/2024: <https://www.ct.ingv.it/index.php/monitoraggio-e-sorveglianza/prodotti-del-monitoraggio/bollettini-settimanali-multidisciplinari/918-bollettino-Settimanale-sul-monitoraggio-vulcanico-geochimico-e-sismico-del-vulcano-Stromboli-del-2024-07-09/file>, last access: 19 August 2024.

484 INGV Bulletin of 16/07/2024: <https://www.ct.ingv.it/index.php/monitoraggio-e-sorveglianza/prodotti-del-monitoraggio/bollettini-settimanali-multidisciplinari/920-bollettino-Settimanale-sul-monitoraggio-vulcanico-geochimico-e-sismico-del-vulcano-Stromboli-del-2024-07-16/file>, last access: 19 August 2024.

487 James, M. R., Lane, S. J., and Chouet, B. A.: Gas slug ascent through changes in conduit diameter: Laboratory insights into a volcano-seismic source process in low-viscosity magmas, *J. Geophys. Res.: Solid Earth*, 111, <https://doi.org/10.1029/2005JB003718>, 2006.

490 Kim, K., and Lees, J. M.: Local Volcano Infrasound and Source Localization Investigated by 3D Simulation, *Seismol. Res. Lett.*, 85, <https://doi.org/10.1785/0220130135>, 2014.

492 Legrand, D., and Perton, M.: What are VLP signals at Stromboli volcano? *J. Volcanol. Geotherm. Res.*, 421, <https://doi.org/10.1016/j.jvolgeores.2021.107429>, 2022.

494 Longo, R., Lacanna, G., Innocenti, L., and Ripepe, M.: Artificial Intelligence and Machine Learning Tools for Improving Early Warning Systems of Volcanic Eruptions: The Case of Stromboli, *IEEE Trans. Pattern Anal. Mach. Intell.*, 46(12), 7973–7982, <https://doi.org/10.1109/TPAMI.2024.3399689>, 2024.

497 Marchetti, E., and Ripepe, M.: Stability of the seismic source during effusive and explosive activity at Stromboli Volcano, *Geophys. Res. Lett.*, 32, <https://doi.org/10.1029/2005GL023962>, 2005.

499 Marchetti, E., Genco, R., and Ripepe, M.: Ground deformation and seismicity related to the propagation and drainage of the dyke feeding system during the 2007 effusive eruption at Stromboli volcano (Italy), *J. Volcanol. Geotherm. Res.*, 182, <https://doi.org/10.1016/j.jvolgeores.2009.01.029>, 2009.

502 McKee, K. F., Roman, D. C., Waite, G. P., and Fee, D.: Silent very long period seismic events (VLPs) at Stromboli Volcano, Italy, *Geophys. Res. Lett.*, 49(23), e2022GL100735, <https://doi.org/10.1029/2022GL100735>, 2022.

504 McNutt, S. R., and Nishimura, T.: Volcanic tremor during eruptions: Temporal characteristics, scaling and constraints on conduit size and processes, *J. Volcanol. Geotherm. Res.*, 178, <https://doi.org/10.1016/j.jvolgeores.2008.07.023>, 2008.

506 Pino, N. A., Moretti, R., Allard, P., and Boschi, E.: Seismic precursors of a basaltic paroxysmal explosion track deep gas accumulation and slug upraise, *J. Geophys. Res.: Solid Earth*, 116, <https://doi.org/10.1029/2011JB008547>, 2011.

508 Pistolesi, M., Delle Donne, D., Pioli, L., Rosi, M., and Ripepe, M.: The 15 March 2007 explosive crisis at Stromboli volcano, Italy: Assessing physical parameters through a multidisciplinary approach, *J. Geophys. Res.*, 116, <https://doi.org/10.1029/2011JB008527>, 2011.



511 Ripepe, M.: Evidence for gas influence on volcanic seismic signals recorded at Stromboli, *J. Volcanol. Geotherm. Res.*, 70,
512 https://doi.org/10.1016/0377-0273(96)00033-8, 1996a.

513 Ripepe, M., Poggi, P., Braun, T., and Gordeev, E.: Infrasonic waves and volcanic tremor at Stromboli, *Geophys. Res. Lett.*,
514 23, https://doi.org/10.1029/96GL02394, 1996b.

515 Ripepe, M., and Gordeev, E.: Gas bubble dynamics model for shallow volcanic tremor at Stromboli, *J. Geophys. Res.: Solid*
516 *Earth*, 104, https://doi.org/10.1029/1998JB900046, 1999.

517 Ripepe, M., Delle Donne, D., Lacanna, G., Marchetti, E., and Ulivieri, G.: The onset of the 2007 Stromboli effusive eruption
518 recorded by an integrated geophysical network, *J. Volcanol. Geotherm. Res.*, 182(3-4), 131–136,
519 https://doi.org/10.1016/j.jvolgeores.2009.02.011, 2009.

520 Ripepe, M., Delle Donne, D., Genco, R., Maggio, G., Pistolesi, M., Marchetti, E., Lacanna, G., Ulivieri, G., and Poggi, P.:
521 Volcano seismicity and ground deformation unveil the gravity-driven magma discharge dynamics of a volcanic eruption, *Nat.*
522 *Commun.*, 6(1), 6998, https://doi.org/10.1038/ncomms7998, 2015.

523 Ripepe, M., Pistolesi, M., Coppola, D., Delle Donne, D., Genco, R., Lacanna, G., ... and Valade, S.: Forecasting effusive
524 dynamics and decompression rates by magmastic model at open-vent volcanoes, *Sci. Rep.*, 7,
525 https://doi.org/10.1038/s41598-017-00748-4, 2017.

526 Ripepe, M., Lacanna, G., Pistolesi, M., Silengo, M. C., Aiuppa, A., Laiolo, M., ... and Delle Donne, D.: Ground deformation
527 reveals the scale-invariant conduit dynamics driving explosive basaltic eruptions, *Nat. Commun.*, 12, 1683,
528 https://doi.org/10.1038/s41467-021-21862-y, 2021a.

529 Ripepe, M., Delle Donne, D., Legrand, D., Valade, S., and Lacanna, G.: Magma pressure discharge induces very long period
530 seismicity, *Sci. Rep.*, 11, https://doi.org/10.1038/s41598-021-86061-x, 2021b.

531 Ripepe, M., and Lacanna, G.: Volcano generated tsunami recorded in the near source, *Nat. Commun.*, 15,
532 https://doi.org/10.1038/s41467-024-18567-x, 2024.

533 Rizzo, A. L., Federico, C., Inguaggiato, S., Sollami, A., Tantillo, M., Vita, F., ... and Grassa, F.: The 2014 effusive eruption at
534 Stromboli volcano (Italy): Inferences from soil CO₂ flux and ³He/⁴He ratio in thermal waters, *Geophys. Res. Lett.*, 42,
535 https://doi.org/10.1002/2015GL064152, 2015.

536 Rosi, M., Bertagnini, A., Harris, A. J. L., Pioli, L., Pistolesi, M., and Ripepe, M.: A case history of paroxysmal explosion at
537 Stromboli: Timing and dynamics of the April 5, 2003 event, *Earth Planet. Sci. Lett.*, 243,
538 https://doi.org/10.1016/j.epsl.2006.01.035, 2006.

539 Rosi, M., Pistolesi, M., Bertagnini, A., Landi, P., Pompilio, M., and Di Roberto, A.: Chapter 14 Stromboli volcano, Aeolian
540 Islands (Italy): present eruptive activity and hazards, *Geol. Soc., London, Mem.*, 37, https://doi.org/10.1144/M37.14, 2013.

541 Sparks, R. S. J.: Dynamics of magma degassing, *Geol. Soc., London, Spec. Publ.*, 213,
542 https://doi.org/10.1144/GSL.SP.2003.213.01.07, 2003.

543 Suckale, J., Keller, T., Cashman, K. V., and Persson, P.-O.: Flow-to-fracture transition in a volcanic mush plug may govern
544 normal eruptions at Stromboli, *Geophys. Res. Lett.*, 43, https://doi.org/10.1002/2016GL068082, 2016.



545 Wang, S.: Finite-difference time-domain approach to underwater acoustic scattering problems, *J. Acoust. Soc. Am.*, 99,
546 <https://doi.org/10.1121/1.414620>, 1996.